ACS APPLIED MATERIALS & INTERFACES

Research Article

www.acsami.org

VO_2 Nanoflakes as the Cathode Material of Hybrid Magnesium–Lithium-Ion Batteries with High Energy Density

Cunyuan Pei,[†] Fangyu Xiong,[†] Jinzhi Sheng,[†] Yameng Yin,[†] Shuangshuang Tan,[†] Dandan Wang,[‡] Chunhua Han,[†] Qinyou An,*[,†] and Liqiang Mai*[,†,§]

[†]State Key Laboratory of Advanced Technology for Materials Synthesis and Processing, Wuhan University of Technology, Hubei, Wuhan 430070, China

[‡]Department of Materials Science and Engineering, University of Michigan, Ann Arbor, Michigan 48109, United States

[§]Department of Chemistry, University of California, Berkeley, California 94720, United States

Ⓢ *Supporting Information*

ABSTRACT: The hybrid magnesium–lithium-ion batteries (MLIBs) combining the dendrite-free deposition of the Mg anode and the fast Li intercalation cathode are better alternatives to Li-ion batteries (LIBs) in large-scale power storage systems. In this article, we reported hybrid MLIBs assembled with the VO_2 cathode, dendrite-free Mg anode, and the Mg–Li dual-salt electrolyte. Satisfactorily, the VO_2 cathode delivered a stable plateau at about 1.75 V, and a high specific discharge capacity of 244.4 mA h g^{-1}. To the best of our knowledge, the VO_2 cathode displays the highest energy density of 427 Wh kg^{-1} among reported MLIBs in coin-type batteries. In addition, an excellent rate performance and a wide operating temperature window from 0 to 55 °C have been obtained. The combination of VO_2 cathode, dual-salt electrolyte, and Mg anode would pave the way for the development of high energy density, safe, and low-cost batteries.

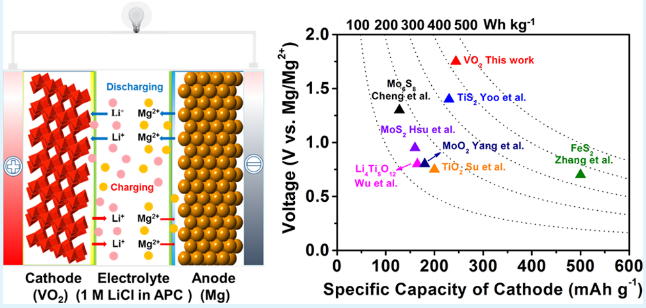

KEYWORDS: *hybrid Mg–Li battery, VO_2, nanoflakes, dendrite-free, APC–LiCl electrolyte, high energy density*

INTRODUCTION

The demand for high energy density batteries is constantly increasing from the viewpoint of renewable energy and environmental problems.[1−3] Among existing battery systems, lithium-ion batteries (LIBs) have received significant attention and achieved great progress over the past few decades. Owing to the advantages of high energy density and long cycle life, LIBs have been used for electric vehicles, portable electronic devices, and other types of applications.[4−7] In general, lithium metal is a perfect anode due to its high theoretical gravimetric capacity (3861 mA h g^{-1}) and the lowest deposition potential (−3.04 V). Unfortunately, Li metal anodes suffer from serious safety issues due to the Li dendritic growth, especially at a high rate discharge-charge conditions. On the other hand, the energy density of commercial LIBs is restrained by the low capacity of graphite anodes (372 mA h g^{-1}).[8−11] In this regard, magnesium ion batteries (MIBs) have attracted considerable interest in terms of research and development in recent years and have been treated as one of the most promising alternatives to LIBs due to the dendrite-free nature of the Mg metal anode.[12−14] Moreover, compared with Li, Mg not only possesses high abundance in the earth's crust (300 times more than Li) but also exhibits several unique characteristics, such as a high theoretical volumetric capacity, which is 1.86 times that of Li (Mg is 3833 mA h cm^{-3} and Li is 2061 mA h cm^{-3}), relatively low toxicity, and high chemical stability when exposed to moisture and the oxygen environment.[15] In addition, when a suitable electrolyte (All-phenyl complex (APC)) was used, the deposition/stripping efficiency of Mg is close to 100%.[16−18] Despite all of the advantages of the Mg anode, the development of MIBs is still full of challenges, which needed to be resolved.[19] For instance, one of the most challenging barriers is that the divalent Mg^{2+} ion shows a strong polarization effect, which dramatically caused the sluggish kinetics of Mg^{2+} ion diffusion and an inactive nature in cathode hosts.[20−23] Although most successful MIBs based on Mo_6S_8 (despite its low voltage and low discharge capacity) have been reported, the development of both high voltage cathode hosts and wide electrochemical window electrolytes is slow.[20,24]

To avoid the limitations of LIBs and MIBs, the concept of Daniell-type batteries, which combine the mature cathode materials from LIBs with the stable Mg solid metal anode in the Mg–Li dual-salt electrolyte has been presented.[25,26] The design integrates a high working voltage, fast Li^+ ion intercalation cathode, and a dendrite-free, low-cost Mg anode in a battery. Remarkable activity and high anodic stability of about 3.0 V (vs

Received: February 21, 2017
Accepted: May 3, 2017
Published: May 3, 2017

DOI: 10.1021/acsami.7b02480
ACS Appl. Mater. Interfaces 2017, 9, 17060−17066

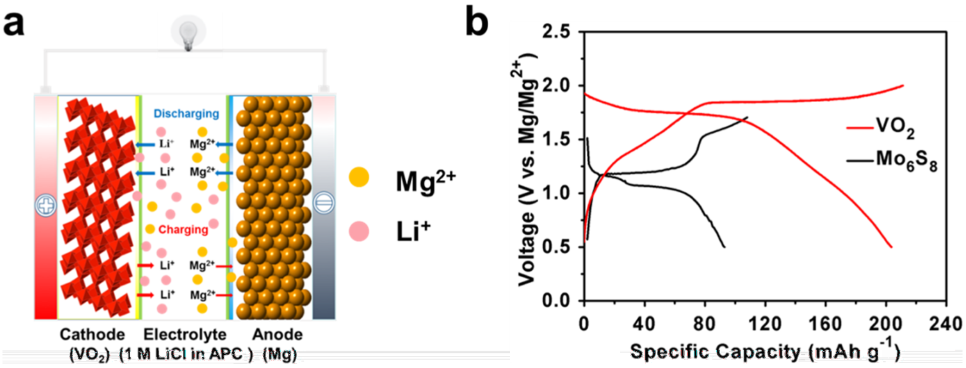

Figure 1. (a) Schematic illustration of the operation mechanism of MLIBs. The cell is discharged with Li ions intercalated into the VO_2 cathode and Mg ions dissolved from the Mg anode. During charging, the reverse takes place. (b) Voltage profiles of the MLIB (VO_2 cathode, Mg anode, and 1 M LiCl in 0.25 M APC electrolyte) at 100 mA g^{-1} and MIB (Mo_6S_8 cathode, Mg anode, and 0.25 M APC) at 20 mA g^{-1}.

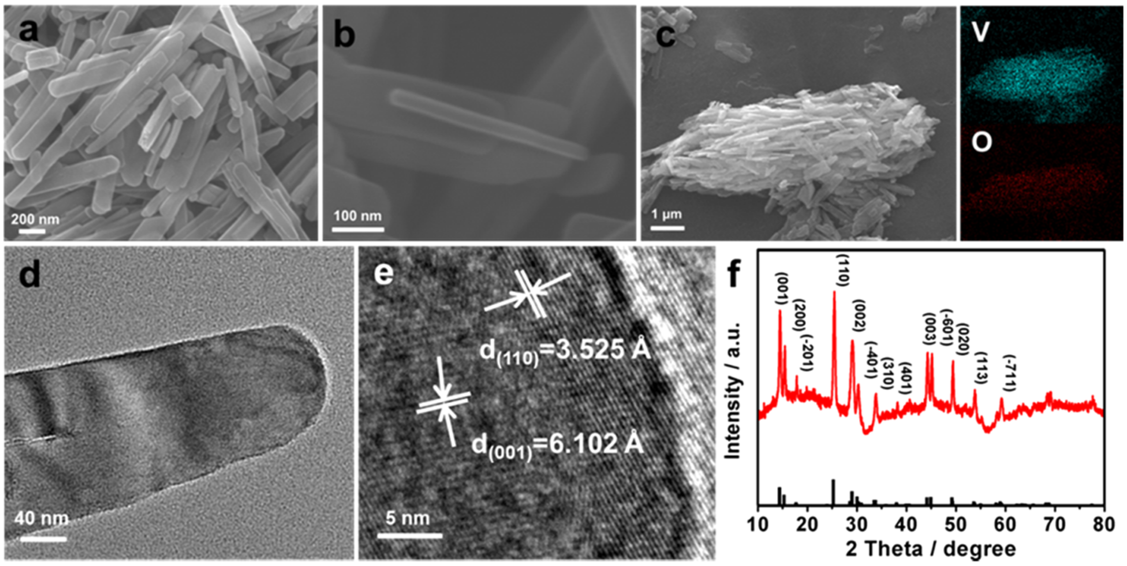

Figure 2. (a–c) FESEM images and elemental mapping images of the prepared VO_2 nanoflakes, (d–e) TEM images, and (f) XRD patterns of VO_2.

Mg/Mg^{2+}) in the APC electrolyte have been reported. The addition of LiCl as a lithium source in APC can not only preserve the electrochemical properties of APC but also keep the Mg anode from forming a passivation film (since the anion Cl^- is a large portion of the APC electrolyte).[27−29] However, the anodic stability of APC is limited to ≤2.0 V (vs Mg/Mg^{2+}) in a stainless steel coin battery due to the corrosion reaction. Given these considerations, many researchers have paid attention to the development of suitable cathodes for practical use.

VO_2 with a suitable voltage plateau (about 2.5 V vs Li/Li^+ and 1.75 V vs Mg/Mg^{2+}) is a promising high energy density cathode in magnesium−lithium-ion batteries (MLIBs). For this purpose, hybrid Mg^{2+}/Li^+ coin cells with VO_2 as the cathode, Mg metal as the anode, and APC−LiCl as the electrolyte, have been designed and assembled. The working mechanism of the hybrid MLIBs is shown in Figure 1a. In the discharging process, Mg^{2+} ions dissolved from the Mg anode and Li^+ ions intercalated into the VO_2 cathode. Whereas during charging, the reverse takes place. As shown in Figure 1b, VO_2 delivers a high working voltage of ∼1.75 V, which is about 0.55 V higher than the most studied MIBs cathode (Mo_6S_8), and a high specific capacity of ∼205 mA h g^{-1}, which is about twice that of Mo_6S_8. Moreover, the VO_2 cathode displays excellent adaptability over a wide temperature range. In addition, the reaction mechanism of VO_2 as a cathode for MLIBs has been investigated via ex situ X-ray diffraction (XRD), transmission electron microscopy (TEM), and so on.

■ RESULTS AND DISCUSSION

The morphology and detailed microstructures of VO_2 were investigated through field-emission scanning electron microscopy (FESEM) and TEM. As shown in FESEM images (Figure 2a−b), the VO_2 samples are composed of uniform nanoflakes, with ∼100 nm in width, hundreds of nanometers in length, and ∼20 nm in thickness. The existence and equal distribution of V and O in the VO_2 nanoflakes have been observed in energy dispersive spectroscopy (EDS) element mapping images (Figure 2c). The stack of nanoflakes is shown in the TEM image of the VO_2 sample (Figure S2), corresponding well with the FESEM images. In the high-resolution TEM (HRTEM) image (Figure 2e) taken from an edge of a single nanoflake (Figure 2d), the lattice fringes are clearly observed with a spacing of 6.102 and 3.525 Å, which correspond to the (001) and (110) lattice planes of VO_2, respectively. XRD has been performed to examine the crystal structure of the VO_2 nanoflakes (Figure 2f); all of the diffraction peaks are consistent with monoclinic VO_2 (JCPDS No. 01-081-2392, space group:

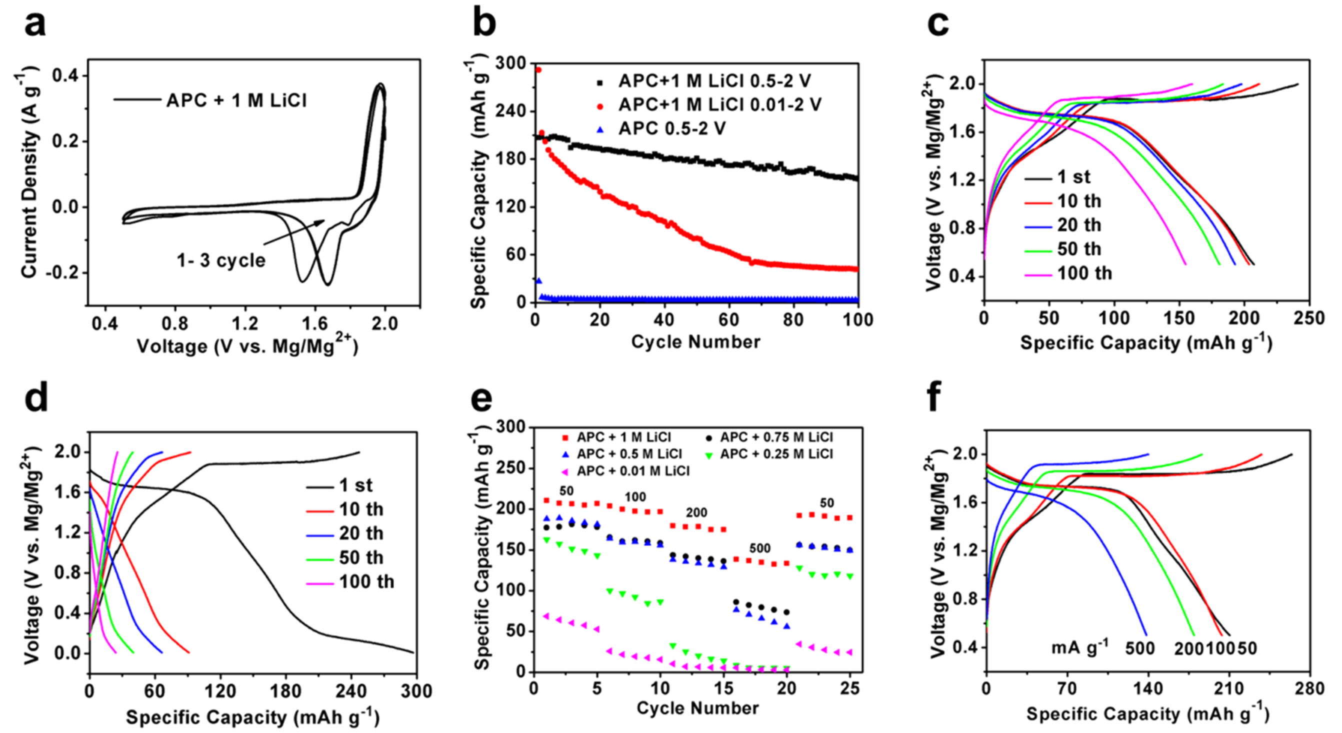

Figure 3. (a) CV curves of VO_2 cathode assembled in MLIB at the scan rate of 0.1 mV s^{-1}. (b) Cycling performance of the VO_2 cathode in MLIB with different electrochemical windows and the VO_2 cathode in MIB at 20 mA g^{-1}. (c, d) Charge−discharge profiles of MLIB between the voltage windows of 0.5−2 and 0.01−2 V, respectively. (e) Rate capability of the VO_2 cathode. (f) Charge−discharge curves of VO_2 at various current densities.

$C2/m$, a = 12.0930 Å, b = 3.7021 Å, c = 6.4330 Å). No peaks of any other phase were detected, indicating the high purity of VO_2, and the sharp diffraction peaks imply the good crystallinity of the VO_2 nanoflakes.

Coin-type batteries with metallic magnesium as the anode and APC−LiCl as the electrolyte were assembled to investigate the electrochemical performance of the VO_2 cathode. First, the cyclic voltammogram (CV) curves of the MLIBs were measured at a scan rate of 0.1 mV s^{-1} in the potential range from 0.5 to 2.0 V versus Mg/Mg^{2+} (Figure 3a). In the subsequent curves after the first cycle, the shapes are almost identical, which indicate the high reversibility of the lithium intercalation/deintercalation. Only one pair of defined redox peaks at 1.9/1.75 V can be observed, corresponding to the charge−discharge voltage profiles (Figure 3c). The CV curves of VO_2 with pure APC electrolyte exhibit no obvious cathodic and anodic peaks (Figure S3a), corresponding well with the charge/discharge curves in Figure S3b, indicating the insertion/extraction of small amounts of Mg^{2+} in the VO_2 cathode (Figure 3b). Furthermore, the charge/discharge curves of the VO_2|APC−LiCl|Mg hybrid battery (0.5−2 V) and VO_2|1 M $LiPF_6$/EC + DMC + EMC (volume ratio of 1:1:1)|Li LIB (1.2−2.7 V) at the same current density of 100 mA g^{-1} are shown in Figure S3c; the fact that Li^+ intercalation/deintercalation dominates the cathode reaction in MLIBs can be confirmed by the similar shape, especially at the plateau.[30] The slight difference, perhaps, is contributed by the difference in Li^+ ion intercalation/deintercalation properties between the electrolyte systems. Because the electrochemical performance is closely associated with the impedance of a cell, the electrochemical impedance spectroscopy of the VO_2 electrode is also measured to support the superior performance. The Nyquist plots of VO_2|APC−LiCl|Mg and VO_2|APC|Mg batteries show a depressed semicircle in the high-frequency region and a straight line in the low-frequency region (Figure S4). The size of the semicircle is associated with the charge transfer impedance (R_{ct}) and the straight line is related to the Warburg impedance (W). In the comparison of these two different systems, the R_{ct} of the VO_2|APC−LiCl|Mg system is much smaller than that of the VO_2|APC|Mg system. Furthermore, the W, which mainly corresponds to the diffusion of ions in the cathode indicates the diffusion of Li^+ ions is much faster than that of the Mg^{2+} ions in the VO_2 cathode, which results in Li^+ ions dominating the intercalation on the cathode side.

The cycling performance and the corresponding charge−discharge curves of VO_2 between different voltage windows are shown in Figure 3b−d. At the current density of 100 mA g^{-1}, the initial discharge capacity of 291.9 mA h g^{-1} is obtained in the voltage window of 0.01−2 V, however, the capacity fast fades to 41.8 mA h g^{-1} (14% of its initial value) after 100 cycles. The severe decrease of discharge capacity can be attributed to the reaction between the voltages of 0.01−0.5 V (Figure 3d), which is irreversible because excessive insertion of Li^+ causes damage of VO_2 structures and further results in the shape change of plateaus (from flat to slope) during cycling at ∼1.75 V (corresponding to ∼2.5 V in LIBs).[31] Meanwhile, in the voltage between 0.5 and 2 V, the VO_2 cathode exhibits a discharge capacity of 206.8 mA h g^{-1} (despite being lower than 291.9 mA h g^{-1}), with enhanced cycling stability, such that a remarkable capacity of 154.9 mA h g^{-1} (75%) was retained after 100 cycles, which is much better than that in 0.01−2 V. The fast decay of the discharge capacity of VO_2|THF−LiCl|Li battery is probably caused by the poor incompatibility of the Li metal and the electrolyte system (Figure S5a). Besides, the Coulombic efficiencies in the two different voltage windows

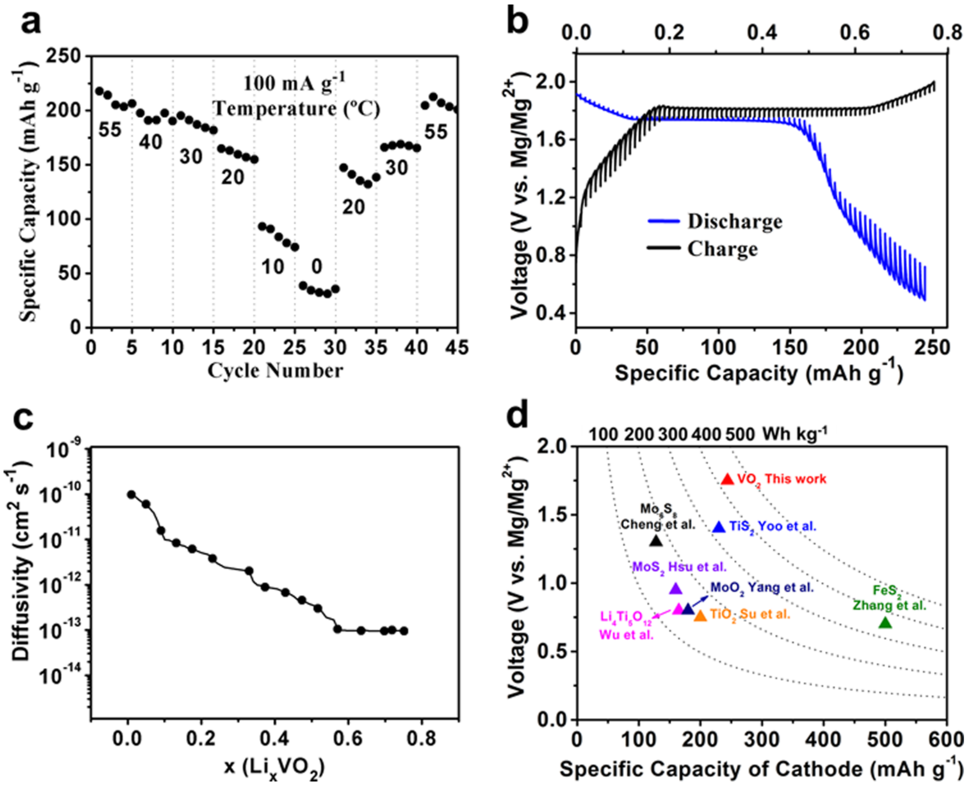

Figure 4. (a) Discharge capacity at different temperatures between 0 and 55 °C at 100 mA g^{-1}. (b) The galvanostatic intermittent titration technique (GITT) curves. (c) Li-ion diffusivity vs the state of discharge. (d) Specific energy density comparison of MLIBs. VO_2 in this work compared to that in previous works, without considering the mass of the solvents.

remained at about 100% (Figure S5b,c) except for the first few cycles, which indicates good reversibility.

In addition, the influence of LiCl concentration on the electrochemical performance of the VO_2 was investigated with the APC electrolyte involving different amounts of LiCl (0.01, 0.25, 0.5, 0.75, and 1 M). Obviously, VO_2 exhibits a better rate capability with the increasing amount of LiCl (Figure 3e,f). As Chen et al. reported,[32] the salt concentration is a trade-off between solubility, ionic conductivity, and viscosity. The increase in lithium solubility results in the change of the ionic conductivity, viscosity, and Li^+ mobility. Definite values of concentration, viscosity, and conductivity in the LiTFSA/AN system have been provided in the work of Yamada et al.[33] With the increasing concentration of Li^+, the declining trend in the value of conductivity decreases. When the concentration of LiCl increased from 0.5 to 0.75 M, the raised viscosity in the electrolyte results in low conductivity and has a negative effect on electrochemical performance. However, the increased Li^+ transference number offsets the negative effect caused by high viscosity. So, after the influence of all factors, the electrolyte systems show a similar result in terms of rate performance. In the high-concentration region, the effect of the increased Li^+ transference number in the electrolyte counteracts the effect of low conductivity, so when the LiCl concentration is 1 M, the rate performance is obviously superior to that at 0.75 M. When the LiCl concentration is 1 M, with the current density increasing from 50 to 100, 200, and 500 mA g^{-1}, the VO_2 cathode delivers discharge capacities of 210.6, 203.7, 179.6, and 138.3 mA h g^{-1}, respectively. Even though the current density is changed from 500 to 50 mA g^{-1}, the cathode shows a stable capacity and the retentive efficiency of the capacity remained at 91.1%, exhibiting excellent rate reversibility. The rate capability of the intercalation electrode material relates to the kinetics of the ion intercalation/deintercalation process, which depends on both the electron transport and ion diffusion velocity/length. In the hybrid system, the high capacity can also be attributed to the effect of the Cl^- anion (effect on anodic stability) and high Li^+ ion concentration (Li^+ transference number).[34,35]

To further investigate their potential application at high and low temperatures, the electrochemical performance of the VO_2 cathode has been studied in an environmental chamber. When the temperature is increased to 55 °C, a high initial discharge capacity of ∼220 mA h g^{-1} is demonstrated, which is higher than the 206.8 mA h g^{-1} obtained at room temperature (Figure 4a). Even at 0 °C, the cell can display a reversible capacity of 35 mA h g^{-1}. The discharge capacity decreases progressively with decrease in temperature, which can be attributed to the slower diffusion of Li^+ ions at a lower temperature. When the temperature was reset to 55 °C after 40 cycles, the capacity immediately returned to 204.7 mA h g^{-1}. A VO_2 cathode exhibiting such a broad working temperature range has not been reported for hybrid MLIBs, to the best of our knowledge.

To scrutinize the source of high discharge capacity and broad temperature adaptability, the kinetics of Li^+ solid-state diffusion in the VO_2 cathode were investigated via the GITT.[36,37] The GITT method reveals ion diffusivity into the composition-dependent electrode kinetics. In Figure 4b, the VO_2 cathode delivers a specific capacity of 244.4 mA h g^{-1} in the GITT measurement, which corresponds to the discharge product of Li_xVO_2 ($x = 0.78$). Moreover, the Li^+ diffusivity (D^{GITT}) can be obtained through the potential response to a low current pulse (20 mA g^{-1}) via the formula (more details can be found in Figure S6 and Scheme 1 in the Supporting Information)[38]

$$D^{\mathrm{GITT}} = \frac{4}{\pi\tau}\left(\frac{m_{\mathrm{B}}V_{\mathrm{M}}}{M_{\mathrm{B}}S}\right)^2\left(\frac{\Delta E_s}{\Delta E_\tau}\right)^2$$

Figure 4c shows that the Li^+ diffusivity decreases from 9.7×10^{-11} to 8.5×10^{-14} cm^2 s^{-1} with the Li concentration increase in the cathode, which may be ascribed to the Coulomb interaction between Li^+ ions. The average Li diffusivity of the VO_2 cathode during the entire intercalation process is $\sim 9.84 \times 10^{-12}$ cm^2 s^{-1}. In comparison, the kinetics of Mg^{2+} solid-state diffusion in the VO_2 cathode was also determined (Figure S7). The average Mg^{2+} diffusivity in VO_2 over the entire intercalation process is $\sim 6.35 \times 10^{-15}$ cm^2 s^{-1}, which is more than 3 orders of magnitude slower than Li^+ diffusivity. The GITT results also indicate that the Li^+ ions dominate the intercalation on the cathode side. Furthermore, the operation voltage and discharge capacity of previous hybrid MLIBs in coin-type batteries have been calculated to compare the energy density to that in our work (Figure 4d). All of the energy densities are just based on the weight of cathode material. The energy density of MLIBs in this work is 427 Wh kg^{-1}, much higher than that of previous MLIBs in coin cells (all at low current density). The energy density of MLIBs at each current density is shown in Figure S8, in terms of energy density, the VO_2 cathode in our work demonstrates the best performance among the reported MLIBs.

The Li ion storage mechanism of VO_2 as a cathode for hybrid MLIBs has been investigated via ex situ XRD and TEM techniques. The XRD patterns of VO_2 at various states of the first cycle are shown in Figure 5a. In the magnified patterns of (001) peaks (Figure 5b), slight shifts can be observed during Li^+ ion intercalation/deintercalation. In the first cycle, when discharged to 1.7, 1, and 0.5 V, the peak shifts to a lower degree, indicating a slight increase of interlayer spacing, which perhaps resulted from the intercalation of lithium ions.[30] When recharged to 1, 1.5, 1.84, and 2 V, the peak exhibits no evidence of shift back to the higher degree, which may be caused by the expansion of the interlayer spacing due to the remaining Li ions in VO_2, corresponding to the initial Coulombic efficiency of about 85%. Only a slight difference was found between XRD patterns of the VO_2 cathode before cycling and after 50 cycles, implying a stable structure of VO_2 during the charge−discharge process.

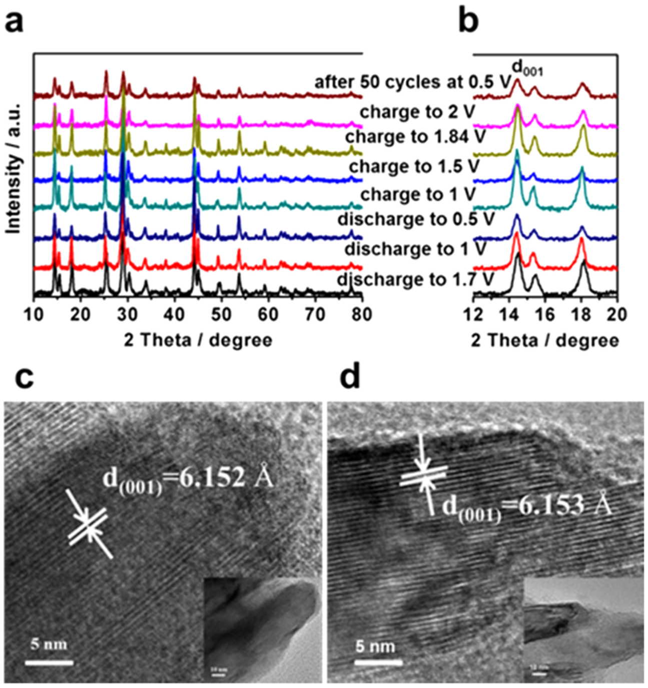

Figure 5. (a, b) Ex situ XRD patterns of VO_2 at various states. (c, d) TEM images of VO_2 discharged to 0.5 V and after 50 cycles at 0.5 V, respectively.

The HRTEM images of VO_2 cathode discharged to 0.5 V in the first cycle and after 50 cycles are displayed in Figure 5c,d, respectively. When discharged to 0.5 V in the first cycle and after 50 cycles, the (001) interlayer spacing was expanded from 6.102 Å (Figure 2e) to 6.152 and 6.153 Å, respectively, which is consistent with the ex situ XRD results. The expanded interlayer spacing of VO_2 is stable and beneficial for ion diffusion and thus increases Li^+ storage performance. The SEM images of the Li anode are shown in Figure S9. Compared with that of LIBs, the most important merit of MLIBs is their dendrite-free deposition on the Mg anode during cycles. To investigate the Mg deposition/stripping on the Mg metal anode, the SEM images of the Mg anode at various charge−discharge states were characterized (Figure S10). As shown in Figure S10a−h, the trend of having a rugged morphology grows with the stripping of Mg^{2+} from the Mg anode and also filled holes can be observed with the deposition of Mg^{2+} on the Mg anode. It is noteworthy that no dendritic morphology has been observed on the Mg anode after 100, 150, and 300 cycles (Figure S10i−k).

■ CONCLUSIONS

In summary, we present a high-energy and safe hybrid MLIB based on the VO_2 cathode, Mg anode, and the APC−LiCl dual-salt electrolyte. The VO_2 cathode in MLIBs exhibits a highly stable and flat plateau of ∼1.75 V, and a high specific capacity of 244.4 mA h g^{-1} in the GITT measurement. At the current density of 100 mA g^{-1}, VO_2 nanoflakes exhibit a high discharge capacity of 206.8 mA h g^{-1}, and 75% of the initial capacity is retained after 100 cycles. In terms of high working voltage and specific discharge capacity, the VO_2 cathode delivers the highest energy density (427 Wh kg^{-1}) among the reported MLIBs in coin-type batteries, to the best of our knowledge. Furthermore, the VO_2 nanoflakes show excellent temperature adaptability (∼220 mA h g^{-1} at 55 °C and ∼35 mA h g^{-1} at 0 °C). The excellent electrochemical performance is attributed to the intercalation kinetics of Li^+ ions into the VO_2 cathode. All of the results indicate the promising applications of the VO_2 cathode in MLIBs, which could lead to new opportunities for the development of advanced materials for energy storage devices.

■ ASSOCIATED CONTENT

Ⓢ Supporting Information

The Supporting Information is available free of charge on the ACS Publications website at DOI: 10.1021/acsami.7b02480.

Additional Figures S1−S10; transparent solution of $AlCl_3$ dissolved in THF, APC, and LiCl in APC; TEM images of VO_2 nanoflakes; CV curves of MIB, voltage profiles of hybrid MIB, MLIB, and LIB; the Nyquist plots of MLIB and MIB; cycling performance of LIB and hybrid MLIB between 0.01−2 and 0.5−2 V; the details of the GITT method and the formula; the Mg^{2+} diffusivity versus the state of discharge; the comparison of energy densities of hybrid MLIBs in coin cells; the SEM images of the Li and Mg anodes at various states (PDF)

AUTHOR INFORMATION

Corresponding Authors

*E-mail: anqinyou86@whut.edu.cn (Q.A.).
*E-mail: mlq518@whut.edu.cn (L.M.).

ORCID

Liqiang Mai: 0000-0003-4259-7725

Author Contributions

The manuscript was written with contributions from all authors. All authors have given approval to the final version of the manuscript.

Notes

The authors declare no competing financial interest.

ACKNOWLEDGMENTS

This work was supported by the National Key Research and Development Program of China (2016YFA0202603), the National Natural Science Foundation of China (51521001, 51602239, 51302203), the National Natural Science Fund for Distinguished Young Scholars (51425204), the Hubei Provincial Natural Science Foundation of China (2016CFB267), and the Fundamental Research Funds for the Central Universities (WUT: 2017-zy-008, 2016IVA090, 2017III009, 2017III007). Prof. Liqiang Mai gratefully acknowledges financial support from the China Scholarship Council (No. 201606955096).

REFERENCES

(1) Wu, N.; Lyu, Y. C.; Xiao, R. J.; Yu, X.; Yin, Y. X.; Yang, X. Q.; Li, H.; Gu, L.; Guo, Y. G. A Highly Reversible, Low-Strain Mg-ion Insertion Anode Material For Rechargeable Mg-ion Batteries. *NPG Asia Mater.* **2014**, *6*, No. e120.

(2) Yagi, S.; Ichitsubo, T.; Shirai, Y.; Yanai, S.; Doi, T.; Murase, K.; Matsubara, E. A Concept of Dual-Salt Polyvalent-Metal Storage Battery. *J. Mater. Chem. A* **2014**, *2*, 1144−1149.

(3) Wu, N.; Yin, Y. X.; Guo, Y. G. Size-Dependent Electrochemical Magnesium Storage Performance of Spinel Lithium Titanate. *Chem. - Asian J.* **2014**, *9*, 2099−2102.

(4) Nam, K. W.; Kim, S.; Lee, S.; Salama, M.; Shterenberg, I.; Gofer, Y.; Kim, J. S.; Yang, E.; Chan, S. P.; Kim, J. S.; et al. The High Performance of Crystal Water Containing Manganese Birnessite Cathodes for Magnesium Batteries. *Nano Lett.* **2015**, *15*, 4071−4079.

(5) Yang, Z.; Zhang, J.; Kintner-Meyer, M. C.; Lu, X.; Choi, D.; Lemmon, J. P.; Liu, J. Electrochemical Energy Storage for Green Grid. *Chem. Rev.* **2011**, *111*, 3577−3613.

(6) Dunn, B.; Kamath, H.; Tarascon, J. M. Electrical Energy Storage for the Grid: A Battery of Choices. *Science* **2011**, *334*, 928−935.

(7) Mahmood, N.; Zhu, J.; Rehman, S.; Li, Q.; Hou, Y. Control Over Large-Volume Changes of Lithium Battery Anodes via Active-Inactive Metal Alloy Embedded in Porous Carbon. *Nano Energy* **2015**, *15*, 755−765.

(8) Yao, H. R.; You, Y.; Yin, Y. X.; Wan, L. J.; Guo, Y. G. Rechargeable Dual-Metal-ion Batteries for Advanced Energy Storage. *Phys. Chem. Chem. Phys.* **2016**, *18*, 9326−9333.

(9) Poizot, P.; Laruelle, S.; Grugeon, S.; Dupont, L.; Tarascon, J. M. Nano-Sized Transition-Metal Oxides as Negative-Electrode Materials for Lithium-ion Batteries. *Nature* **2000**, *407*, 496−499.

(10) Etacheri, V.; Marom, R.; Ran, E.; Salitra, G.; Aurbach, D. Challenges in the Development of Advanced Li-ion Batteries: A Review. *Energy Environ. Sci.* **2011**, *4*, 3243−3262.

(11) Zou, F.; Hu, X.; Long, Q.; Li, Z.; Hu, C.; Zeng, R.; Jiang, Y.; Huang, Y. MOF-Derived Porous $ZnO/ZnFe_2O_4/C$ Octahedra with Hollow Interiors for High-Rate Lithium-ion Batteries. *Adv. Mater.* **2014**, *26*, 6622−6628.

(12) Sa, N.; Kinnibrugh, T. L.; Wang, H.; Gautam, G. S.; Chapman, K. W.; Vaughey, J. T.; Key, B.; Fister, T. T.; Freeland, J. W.; Proffit, D. L.; et al. Structural Evolution of Reversible Mg Insertion into a Bilayer Structure of $V_2O_5{\cdot}nH_2O$ Xerogel Material. *Chem. Mater.* **2016**, *28*, 2962−2969.

(13) Wu, N.; Yang, Z. Z.; Yao, H. R.; Yin, Y. X.; Gu, L.; Guo, Y. G. Improving the Electrochemical Performance of the $Li_4Ti_5O_{12}$ Electrode in a Rechargeable Magnesium Battery by Lithium-Magnesium Co-Intercalation. *Angew. Chem., Int. Ed.* **2015**, *54*, 5757−5761.

(14) Wang, L.; Asheim, K.; Vullum, P. E.; Svensson, A. M.; Vullumbruer, F. Sponge-Like Porous Manganese(II,III) Oxide as a Highly Efficient Cathode Material for Rechargeable Magnesium Ion Batteries. *Chem. Mater.* **2016**, *28*, 6459−6470.

(15) Dong, H.; Li, Y.; Liang, Y.; Li, G.; Sun, C. J.; Ren, Y.; Lu, Y.; Yao, Y. A Magnesium-Sodium Hybrid Battery with High Operating Voltage. *Chem. Commun.* **2016**, *52*, 8263−8266.

(16) Gao, T.; Noked, M.; Pearse, A. J.; Gillette, E.; Fan, X.; Zhu, Y.; Luo, C.; Suo, L.; Schroeder, M. A.; Xu, K.; et al. Enhancing the Reversibility of Mg/S Battery Chemistry through Li^+ Mediation. *J. Am. Chem. Soc.* **2015**, *137*, 12388−12393.

(17) Yu, X.; Manthiram, A. Performance Enhancement and Mechanistic Studies of Magnesium-Sulfur (Mg-S) Cells with an Advanced Cathode Structure. *ACS Energy Lett.* **2016**, *1*, 431−437.

(18) Barile, C. J.; Barile, E. C.; Zavadil, K. R.; Nuzzo, R. G.; Gewirth, A. A. Electrolytic Conditioning of a Magnesium Aluminum Chloride Complex for Reversible Magnesium Deposition. *J. Phys. Chem. C* **2014**, *118*, 27623−27630.

(19) Park, M. S.; Kim, J. G.; Kim, Y. J.; Choi, N. S.; Kim, J. S. Recent Advances in Rechargeable Magnesium Battery Technology: A Review of the Field's Current Status and Prospects. *ChemInform* **2015**, *46*, 570−585.

(20) Knight, J. C.; Therese, S.; Manthiram, A. On the Utility of Spinel Oxide Hosts for Magnesium-ion Batteries. *ACS Appl. Mater. Interfaces* **2015**, *7*, 22953−22961.

(21) Duffort, V.; Sun, X.; Nazar, L. F. Screening for Positive Electrodes for Magnesium Batteries: A Protocol for Studies at Elevated Temperatures. *Chem. Commun.* **2016**, *52*, 12458−12461.

(22) Liang, Y.; Feng, R.; Yang, S.; Ma, H.; Liang, J.; Chen, J. Rechargeable Mg Batteries with Graphene-like MoS_2 Cathode and Ultrasmall Mg Nanoparticle Anode. *Adv. Mater.* **2011**, *23*, 640−643.

(23) Liu, B.; Luo, T.; Mu, G.; Wang, X.; Chen, D.; Shen, G. Rechargeable Mg-ion Batteries Based on WSe_2 Nanowire Cathodes. *ACS Nano* **2013**, *7*, 8051−8058.

(24) Shterenberg, I.; Salama, M.; Gofer, Y.; Levi, E.; Aurbach, D. The Challenge of Developing Rechargeable Magnesium Batteries. *MRS Bull.* **2014**, *39*, 453−460.

(25) Ichitsubo, T.; Okamoto, S.; Kawaguchi, T.; Yu, K.; Oba, F.; Yagi, S.; Goto, N.; Doi, T.; Matsubara, E. Toward "Rocking-Chair Type" Mg-Li Dual-Salt Battery. *J. Mater. Chem. A* **2015**, *3*, 10188−10194.

(26) Cheng, Y.; Choi, D.; Han, K. S.; Mueller, K. T.; Zhang, J. G.; Sprenkle, V. L.; Liu, J.; Li, G. Toward the Design of High Voltage Magnesium-Lithium Hybrid Batteries Using Dual-Salt Electrolytes. *Chem. Commun.* **2016**, *52*, 5379−5382.

(27) Pour, N.; Gofer, Y.; Dan, T. M.; Aurbach, D. Structural Analysis of Electrolyte Solutions for Rechargeable Mg Batteries by Stereoscopic Means and DFT Calculations. *J. Am. Chem. Soc.* **2011**, *133*, 6270−6278.

(28) Yoo, H. D.; Shterenberg, I.; Gofer, Y.; Doe, R. E.; Fischer, C. C.; Ceder, G.; Aurbach, D. A Magnesium-Activated Carbon Hybrid Capacitor. *J. Electrochem. Soc.* **2014**, *161*, A410−A415.

(29) Gofer, Y.; Chusid, O.; Gizbar, H.; Viestfrid, Y.; Gottlieb, H. E.; Marks, V.; Aurbach, D. Improved Electrolyte Solutions for Rechargeable Magnesium Batteries. *Electrochem. Solid-State Lett.* **2006**, *9*, A257−A260.

(30) Gao, T.; Han, F.; Zhu, Y.; Suo, L.; Luo, C.; Xu, K.; Wang, C. Hybrid Mg^{2+} /Li^+ Battery with Long Cycle Life and High Rate Capability. *Adv. Energy Mater.* **2014**, *5*, No. 1401507.

DOI: 10.1021/acsami.7b02480

(31) He, G.; Li, L.; Manthiram, A. VO2/rGO Nanorods as a Potential Anode for Sodium and Lithium-ion Batteries. *J. Mater. Chem. A* **2015**, *3*, 14750−14758.

(32) Suo, L.; Hu, Y. S.; Li, H.; Armand, M.; Chen, L. A New Class of Solvent-in-Salt Electrolyte for High-Energy Rechargeable Metallic Lithium Batteries. *Nat. commun.* **2013**, *4*, No. 1481.

(33) Yamada, Y.; Furukawa, K.; Sodeyama, K.; Kikuchi, K.; Yaegashi, M.; Tateyama, Y.; Yamada, A. Unusual Stability of Acetonitrile-Based Superconcentrated Electrolytes for Fast-Charging Lithium-ion Batteries. *J. Am. Chem. Soc.* **2014**, *136*, 5039−5046.

(34) Yoo, H. D.; Liang, Y.; Li, Y.; Yao, Y. High Areal Capacity Hybrid Magnesium-Lithium-ion Battery with 99.9% Coulombic Efficiency for Large-Scale Energy Storage. *Acs Appl. Mater. Interfaces* **2015**, *7*, 7001−7007.

(35) Li, L.; Lu, H.; Deng, K. Single CdSe Nanobelts-on-Electrodes Schottky Junction Solar Cells. *J. Mater. Chem. A* **2013**, *1*, 2089−2093.

(36) Weppner, W.; Huggins, R. A. Determination of the Kinetic Parameters of Mixed-Conducting Electrodes and Application to the System Li_3Sb. *J. Electrochem. Soc.* **1977**, *124*, 1569−1578.

(37) An, Q.; Li, Y.; Yoo, H. D.; Chen, S.; Ru, Q.; Mai, L.; Yao, Y. Graphene Decorated Vanadium Oxide Nanowire Aerogel for Long-Cycle-Life Magnesium Battery Cathodes. *Nano Energy* **2015**, *18*, 265−272.

(38) Deiss, E. Spurious Chemical Diffusion Coefficients of Li^+ in Electrode Materials Evaluated with GITT. *Electrochim. Acta* **2005**, *50*, 2927−2932.

DOI: 10.1021/acsami.7b02480
ACS Appl. Mater. Interfaces 2017, 9, 17060−17066